Frequency behavior of saturated nonlinear function series based on opamps

E. Ortega-Torres and C. Sánchez-López
Universidad Autónoma de Tlaxcala (UAT),
Clzda Apizaquito s/n, km. 1.5, Apizaco, Tlaxcala, 70300, Mexico.

J. Mendoza-López
Microelectronics Institute of Sevilla,
(IMSE-CSIC) and University of Seville, Seville 41092, Spain.

In multiscroll chaotic circuit design based on active devices, piece-wise linear (PWL) approaches are often used to model the behavior of nonlinear functions, thereby that the behavior of a chaotic system can be forecasted through numerical simulations. However, although PWL models are relatively easy to build, they do not include any information related on the performance parameters of the active devices to be used. This a serious shortcoming, since PWL-models introduces a level of inaccuracy into a numerical analysis which is more evident when numerical simulations and experimental results are compared. These differences are more pronounced when the chaotic waveforms to be generated are pushed to operate at high-frequency. This paper introduces experimental results on the frequency behavior of a nonlinear function called saturated nonlinear function series based on operational amplifiers. These new results are key not only on the automatic synthesis of chaotic attractors and on the synchronization schemes used in secure communication systems based on chaos, but also on the metrics used to evaluate the complexity of a chaotic system. A mathematical model to characterize the behavior of the nonlinear function is also derived, showing a better accuracy compared with the PWL approach. The theoretical derivations and related results are experimentally validated through implementations from commercially available devices.

Keywords: Chaotic systems; computer aided analysis; saturated function series; modeling; chaos.

En el diseño de circuitos caóticos con múltiples enrollamientos basado en dispositivos activos, el comportamiento de las funciones no lineales es representado por aproximaciones lineales a trozos (PWL). Sin embargo, aunque modelos PWL son fáciles de construir, estos no incluyen ninguna información relacionada con los parámetros de desempeño de los dispositivos activos a ser usados. Este es un serio inconveniente, ya que modelos PWL introducen un nivel de inexactitud en un análisis numérico el cual llega a ser más evidente cuando las simulaciones numéricas son comparadas con resultados experimentales. Estas diferencias son más pronunciadas cuando las formas de onda caóticas a ser generadas son empujadas a operar en alta frecuencia. Este artículo introduce resultados experimentales sobre el comportamiento en frecuencia de la función no lineal llamada serie de funciones saturadas las cuales son diseñadas con amplificadores operacionales. Los nuevos resultados son clave no solamente en la síntesis automática de atractores caóticos y en los esquemas de sincronización usados en los sistemas de comunicación basados en caos, pero también en las métricas usadas para evaluar la complejidad de un sistema caótico. Un modelo analítico para caracterizar el comportamiento de la función no lineal es derivado y este es más exacto que el modelo PWL. Los resultados teóricos son validados con resultados experimentales a través del uso de dispositivos comerciales.

Descriptores: Sistemas caóticos; análisis asistido por computadora; serie de funciones saturadas; modelado; caos.

PACS: 05.45.Pq; 05.45.Pq; 84.30.Ng; 07.50.Ek; 84.30.-r; 01.50.Pa

1. Introduction

A piece-wise linear (PWL) approach is often used to model the behavior of nonlinear functions [2-5,11,14-19,22,30,33-39,41]. In this sense, the saturated nonlinear function series (SNFS) has been used as the nonlinear part into a chaotic system [14-16,25,26,37,39], so that this can numerically be analyzed and common metrics used to measure the complexity of a nonlinear system can also be applied [2-5,8,11,14-19,22,30,33-39,41]. Moreover, synchronization schemes of chaotic oscillators to be used into a secure communication system have been proposed [3,4,13,23], where a PWL approach is used to model the behavior of the nonlinear function. Therefore, the performance of the synchronization scheme is forecasted through numerical simulations [4,10,23,31]. In practice, however, the SNFS is often designed by stacking several very high-gain voltage operational amplifiers (Opamps) as depicted in Fig. 1 [14-16,25,26,37,39], showing that the real behavior of the SNFS
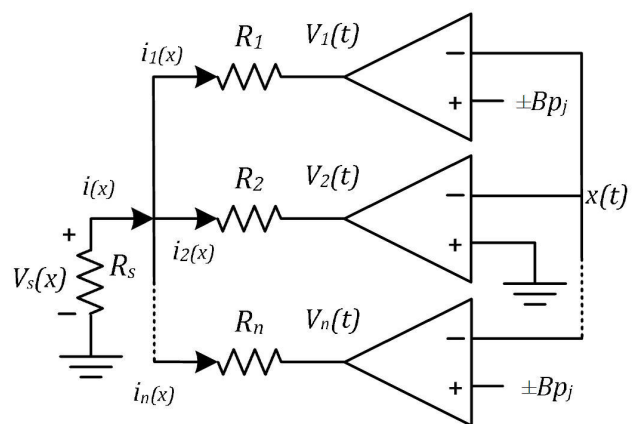

FIGURE 1. SNFS designed with Opamps to generate *n*-plateaus.
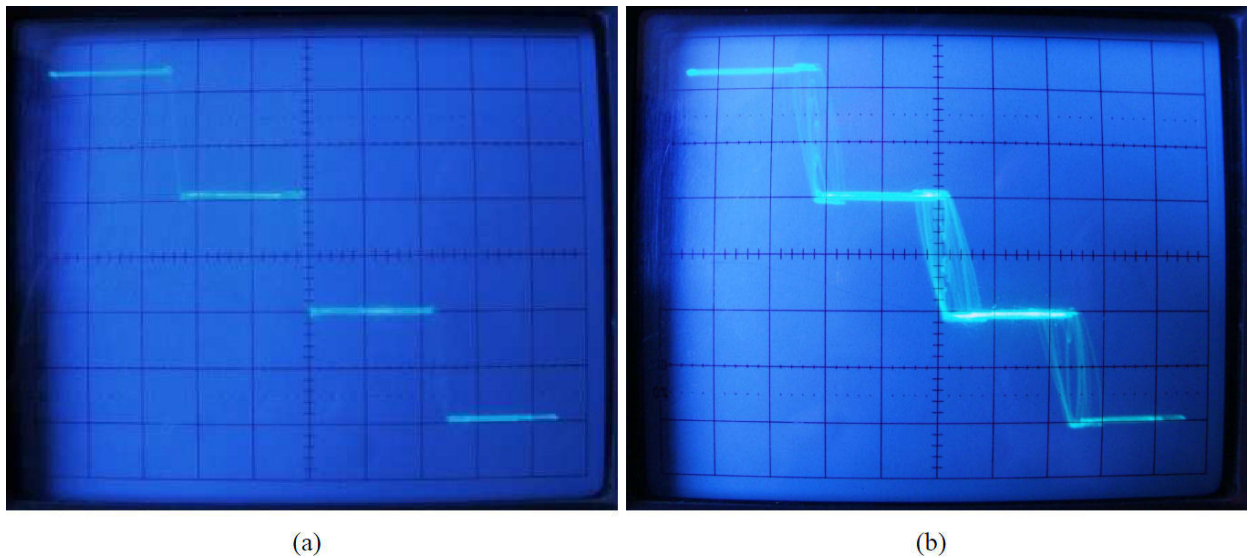
(a)　　　　　　　　　　　　　　　　　(b)

FIGURE 2. Frequency behavior of the SNFS based on Opamps. Vertical axes: $V_s(x)$ (20 mV/div); Horizontal axes: $x(t)$ (2V/div). Operating frequency of $x(t)$ to (a) 450 Hz and (b) 3.45 kHz.

is far different from the PWL model. These differences are more pronounced when the functionality of the SNFS designed with amplifiers is pushed to operate at high frequency, as shown in Fig. 2. This is because PWL models do not reflect the real behavior of a SNFS designed with Opamps, since they are only limited to characterize a static behavior instead of a dynamic behavior. According to Fig. 2(a), the behavior of the SNFS can be well approximated by using a PWL model, since the operating frequency of the chaotic signal $x(t)$, is relatively low (450 Hz). However, if the operating frequency of the chaotic signal is monotonically increased, as shown in Fig. 2(b), the behavior of the SNFS cannot be approximated by using a PWL function, by the reasons above mentioned. It is worth remarking that the operating frequencies of $x(t)$ to 450 Hz and 3.45 kHz were selected in order to show the real behavior of the SNFS, but these values do not have to be the same. Furthermore, from Fig. 1, three Opamps along with their resistors, R_s and the breakpoints (Bp), one by each amplifier given by: $+Bp_1$, 0, $-Bp_1$, were used to obtain Fig. 2, and all they are embedded into a chaotic system, as will be shown in Sec. 5. As a consequence, inaccuracies are introduced not only in the numerical generation of chaotic waveforms [5,11,14-18,25,26,34,37,39,41], but also on the metrics used to evaluate the complexity of nonlinear systems [1,8,9,12,20,27,30,32]. Besides, in chaos synchronization schemes a relatively high level of inaccuracy is also introduced in the numerical simulations and as a result, in practice, a communication system based on chaos might be infeasible [4,10,13,23,31].

This paper introduces the effects that present the SNFS designed with Opamps when the operating frequency of the chaotic signal increases. Note that waveforms of a chaotic oscillator are nearly periodic when the output power is concentrated in a single-frequency component which is centered near the operating frequency of the chaotic oscillator circuit [6,7,21,22,24,28]. Furthermore, the waveforms become chaotic whether the circuit is tuned at its chaotic region of operation. Thus, the power is extended to more frequency components into a bandwidth small, with lower and higher frequencies than the center operating frequency. Moreover, a behavioral model that characterize the real behavior of the SNFS designed with Opamps is also derived, where the most influential performance parameters of an Opamp, like the dynamic range (*DR*), gain bandwidth product (*GB*), DC gain (A_{DC}) and slew-rate (*SR*) are taken into account. In order to validate the proposed nonlinear model of the SNFS, we also compare the behavior of the nonlinear function at high-frequency when a linear model and the proposed nonlinear model of the Opamp are used. As a result, the nonlinear model allows modeling of the SNFS with better accuracy. In this way, the new behavioral model can be used to improve all the disadvantages before mentioned on the use of PWL models. The theoretical derivations are validated through practical implementations by using commercially available devices.

2. Frequency behavior of SNFS

A real Opamp exhibits finite performance parameters that impact directly on the performance of analog circuits, *e.g.*, the SNFS based on Opamps. To demonstrate the real behavior of the SNFS, the chaotic circuit introduced in Ref. 26 has been built and experimentally tested by using the UA741 Opamp, in order to generate chaotic waveforms at 1-D. Therefore, without loss of generality, here simply we consider the circuit shown in Fig. 1 [26], but kept in mind the chaotic circuit in general. Analyzing Fig. 1 and assuming that the positive node of R_s is of low impedance, the output current is given by

$$i(x) \approx \frac{V_1(t)}{R_1} + \frac{V_2(t)}{R_2} + \cdots \frac{V_n(t)}{R_n} \qquad (1)$$
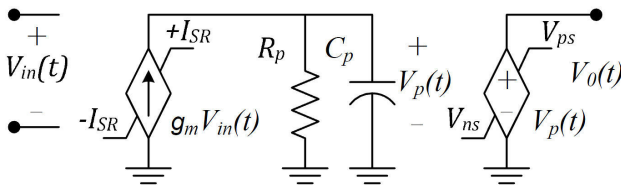
FIGURE 3. Macromodel to characterize the nonlinear behavior of Opamps.

where $V_{1,2,\cdots n}(t) = f(DR, GB, A_{DC}, SR, x(t))$ and $\pm Bp_j$ are computed as in Refs. 25 and 26. Applying a chaotic signal on the *x*-terminal one can obtain the real behavior of the SNFS, where *i(x)* has been indirectly measured across the terminals of $R_s = 100\ \Omega$. Basically, the voltage drop across the terminals of R_s is firstly measured and later *i(x)* is obtained. As above mentioned, three Opamps together with their resistors are used to experimentally generate Fig. 2. Thus, Fig. 2 shows the real behavior of the SNFS with four plateaus at two operating frequencies [6,7,21,28], and the maximum voltage drop across R_s is measured as $V_s(x) \approx 124$ mV and as a consequence, the maximum current is measured as $i(x) \approx 1.24$ mA. As one see, a PWL approach can be used to model the behavior of the SNFS at low frequency, as shown in Fig. 2(a) [14-16,25,26,37,39]. However, when the center frequency of the chaotic signal increases, the PWL model becomes infeasible, as shown in Fig. 2(b). At this stage, it is clear that to palliate all the disadvantages that present the use of PWL models on the application areas before mentioned, a simple and accurate behavioral model that captures these effects is widely demanded. In this context, chaotic system performance characteristics can be evaluated by using a more complex model but with better accuracy for Opamps (*e.g.*, at the transistor level of abstraction), however, it is well-known that complex models are slower. Otherwise, simple models may, however, compromise the accuracy. This trade-off between accuracy and simulation speed is not addressed herein [29], but however, the deduced previously nonlinear models, firstly for Opamps and later on for the SNFS, have a better accuracy than PWL approaches as will be seen throughout the paper. It is worth mentioning that the real effects on the behavior at frequency of the SNFS depicted in Fig. 2(b) is a fundamental problem that has not been examined in the literature, until today. Perhaps the reason of that previous works have not considered the frequency behavior of the nonlinear function of a chaotic system is due to that they have principally been focused to generate numerically chaotic waveforms instead of experimental tests. But even, some experimental results have only been measured at low-frequency where a PWL-model can be used to exactly model the nonlinear function, and therefore, a good accuracy is obtained when experimental results are compared with numerical simulations.

3. Behavioral model of Opamps

In order to build a behavioral model for the SFNS, a behavioral model that mimics the nonlinear behavior of Opamps must be first derived [2]. In this way, Fig. 3 shows the nonlinear macromodel of an Opamp, where the most influential performance parameters are included [2]. Note that the macromodel for Opamps introduced in Ref. 2 uses a nonlinear resistor at the output port contrary to Fig. 3. Simple analysis of Fig. 3 allows obtaining a set of equations of the amplifier model that will be very useful to build the behavioral model of the SNFS. On one hand, when the Opamp operates linearly, its output voltage is governed by the following differential equation

$$\frac{dV_0(t)}{dt} = V_{\text{in}}(t)GB - \frac{V_0(t)GB}{A_{DC}},$$

$$-\frac{SR}{GB} \le V_{\text{in}}(t) \le \frac{SR}{GB} \qquad (2)$$

where

$$g_m = \frac{A_{DC}}{R_p}, \qquad I_{SR} = C_p SR,$$

$$\frac{1}{R_p C_p} = \frac{GB}{A_{DC}},$$

C_p and R_p model the dominant-pole corner frequency. On the other hand, when the input differential voltage exceeds this limit, the Opamp slews and the output voltage evolves according to

$$\frac{dV_0(t)}{dt} = +SR - \frac{V_0(t)GB}{A_{DC}}, \quad +\frac{SR}{GB} < V_{\text{in}}(t)$$

$$\frac{dV_0(t)}{dt} = -SR - \frac{V_0(t)GB}{A_{DC}}, \quad -\frac{SR}{GB} > V_{\text{in}}(t) \qquad (3)$$

Note, however, that the output voltage is limited by the saturation voltages as shown in Fig. 3 and given by

$$V_{\text{ns}} \le V_0(t) \le V_{\text{ps}} \qquad (4)$$

where V_{ps} is the positive saturation voltage, V_{ns} is the negative saturation voltage and the difference of them is well-know as the *DR* of the amplifier.

Relying on the nonlinear model described by (2), (3) and (4), a simple linear model for the Opamp can be deduced [2]. Here, two performance parameters are only included into the linear model, which is given by

$$\frac{dV_0(t)}{dt} = V_{\text{in}}(t)GB - \frac{V_0(t)GB}{A_{DC}} \qquad (5)$$

This linear model along with the nonlinear model of the Opamp will be used to numerically predict the behavior of the SNFS. Both numerical simulations are compared with experimental results, showing that the behavior of the SNFS based on the nonlinear model of the Opamp is more accurate than the linear model, as will be illustrated in Sec. 5.

TABLE I. Performance parameters measurement of the UA741 Opamp.

Parameter	Value	Parameter	Value
A_{DC}	106.82 dB	V_{ps}	9 V
SR	2.2 V/μs	V_{ns}	-9 V
GB	2.72 MHz	V_{dd}	$\pm$11 V

4. Behavioral model of SNFS

Once that the behavioral model of the Opamp has been deduced, the behavioral model of the SFNS can be built. According to Fig. 1, each Opamp must be replaced by (2) and (3) with respect to the operation region, limiting each output voltage by (4) and by including the $\pm Bp_j$ associated to each amplifier. The number of Bp, denoted by j, depends of the number of scrolls to be generated, and the magnitude of the positive and negative breakpoints must be nearly the same in order to obtain symmetry in the generation of the chaotic attractors, for more details see [25,26]. Therefore, at the general case the nonlinear behavior of the SNFS is given by (6). For the linear case, each Opamp must be replaced by (5) and taking into account the $\pm Bp_j$, respectively. Note that $V_{\text{in}}(t) = Bp_j - x(t)$ or $V_{\text{in}}(t) = -Bp_j - x(t)$ is the input signal for each Opamp shown in Fig. 1 and according to each Bp, respectively, where Bp is a DC voltage source which is used to compare if $x(t)$ is larger or smaller than Bp. Thus, (7) is the system of equations for the linear case. Therefore, once that each output voltage is numerically computed, the output current of each system of equations is obtained by using (1). It is important mentioning that (6) and (7) can be used to generate any number of plateaus of a SFNS contrary to the methodologies previously reported, where two PWL functions are required to generate an even or odd number of plateaus and whose negative impact has been above discussed [6,7,14-16,21,25,26,28,37,39]. For instance, in order to achieve a SNFS with four plateaus, the system of equations given by (6) and (7) are governed by three differential equations. Otherwise, a system of equations integrated by four differential equations is required to generate five plateaus. Because (7) and principally (6) have been deduced by considering the performance parameters of the Opamp, they can be obtained either from manufacturer data sheet or experimental measurements. Table I shows the performance parameters of the UA741 Opamp that are used in the experimental tests.

5. Experimental results

To validate the results derived in the previous section, a chaotic waveform with center frequency of 3.45 kHz has been experimentally generated and stored into a file in order to be used as excitation signal in the behavior models of the SNFS previously derived. A SNFS with four plateaus is herein considered with $R_{1,2,3}$=40 kΩ and $\pm Bp_1 = \pm4.5$ V [7,14-16,21,25,26,37,39]. Thus to validate the proposed behavior models, the output waveform obtained from (7) along with (1) is compared with experimental data, as shown in Fig. 4(a). Later on, the output waveform obtained from (6) along with (1) is also compared with experimental data, as shown in Fig. 4(b). We would like to note that the values of the $\pm Bp_1$ are not only responsible of that symmetric chaotic attractors can be generated, but depending of the magnitude of $x(t)$, they also contribute to that the chaotic signal jump from one plateaus to another, as shown in Fig. 2 and Fig. 4.

$$\frac{dV_1(t)}{dt} = p_1 - \frac{V_1(t)GB}{A_{DC}}$$

$$\frac{dV_2(t)}{dt} = p_2 - \frac{V_2(t)GB}{A_{DC}}$$

$$\vdots$$

$$\frac{dV_n(t)}{dt} = p_n - \frac{V_n(t)GB}{A_{DC}}$$

$$, p_n = \begin{cases} +SR & \pm Bp_j - x(t) > +\frac{SR}{GB} \\ (\pm Bp_j - x(t))GB & -\frac{SR}{GB} \le \pm Bp_j - x(t) \le +\frac{SR}{GB} \\ -SR & \pm Bp_j - x(t) < -\frac{SR}{GB} \end{cases} \quad \text{(Nonlinear Model)} \quad (6)$$

$$\frac{dV_1(t)}{dt} = (\pm Bp_j - x(t))GB - \frac{V_1(t)GB}{A_{DC}}$$

$$\frac{dV_2(t)}{dt} = (\pm Bp_j - x(t))GB - \frac{V_2(t)GB}{A_{DC}}$$

$$\vdots$$

$$\frac{dV_n(t)}{dt} = (\pm Bp_j - x(t))GB - \frac{V_n(t)GB}{A_{DC}}$$

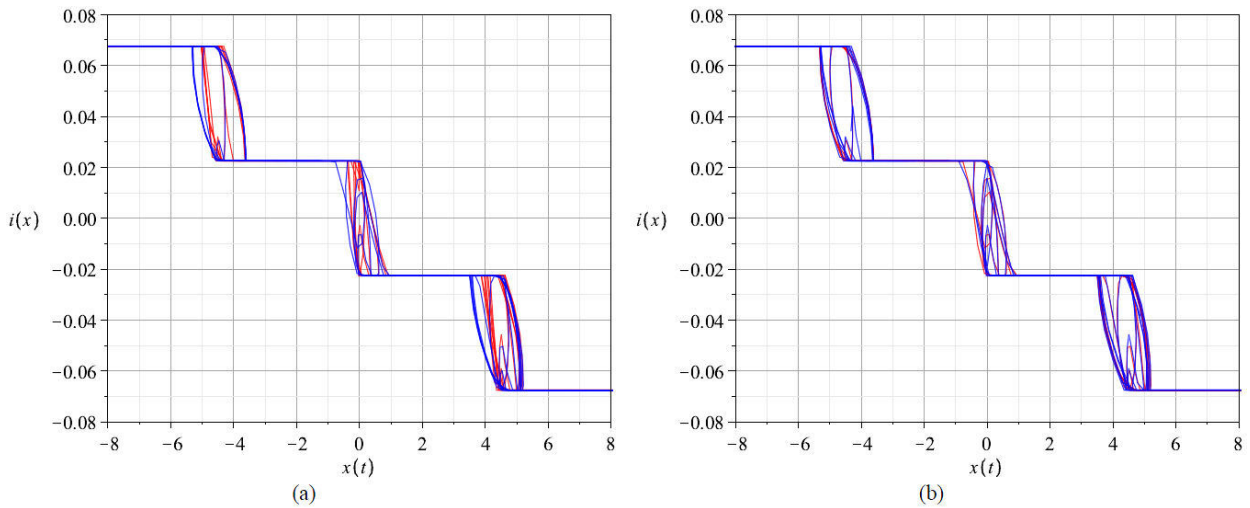$$\text{(Linear Model)} \quad (7)$$

FIGURE 4. Comparison between (Blue line) experimental data and (Red line) behavior models: (a) Linear model, (b) Nonlinear model.
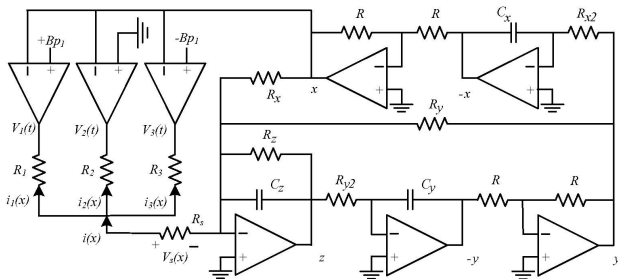

FIGURE 5. Chaotic circuit with the SNFS shown in Fig. 1.

By inspection of Fig. 4(a), the linear model introduces a level of inaccuracy higher than the nonlinear model. According to Fig. 4(b), the response of the proposed nonlinear behavior model is almost equal for the experimental data and hence, this new model can be used not only to improve the automatic synthesis of chaotic attractors [26,28,40] and the synchro-

nization schemes used in communication systems based on chaos [4,10,23,31], but also to realize a better forecast on the common metrics used to evaluate the complexity of nonlinear systems [1,9,12,20,27,32]. In this context and as one can see throughout the paper, the real behavior of the SNFS based on active devices must unavoidably be taken into account in all the topics before mentioned, since whether PWL models are used, a linearization technique is indirectly involved, causing a level of inaccuracy between numerical and experimental results, which become more evident when they are compared at higher frequencies, as shown in Fig. 2 and Fig. 4. These last topics will be addressed in future work. Moreover, the simple block circuit diagram introduced in Ref. 26 is also constructed for generation of multiscroll chaotic attractors at 1-D, as shown in Fig. 5. The SNFS shown in Fig. 1 is used as nonlinear function. Analyzing Fig. 5, the new nonlinear system to be solved is given by

$$\frac{dx(t)}{dt} = \frac{y(t)}{R_{x2}C_x}; \qquad \frac{dy(t)}{dt} = \frac{z(t)}{R_{y2}C_y}; \qquad \frac{dz(t)}{dt} = -\frac{x(t)}{R_xC_z} - \frac{y(t)}{R_yC_z} - \frac{z(t)}{R_zC_z} + \frac{1}{C_z}\left(\frac{V_1(t)}{R_1} + \frac{V_2(t)}{R_2} + \frac{V_3(t)}{R_3}\right)$$

$$\frac{dV_1(t)}{dt} = p_1 - \frac{V_1(t)GB}{A_{DC}}; \qquad \frac{dV_2(t)}{dt} = p_2 - \frac{V_2(t)GB}{A_{DC}}; \qquad \frac{dV_3(t)}{dt} = p_3 - \frac{V_3(t)GB}{A_{DC}}$$

$$p_1 = \begin{cases} +SR & + Bp_1 - x(t) > +\frac{SR}{GB} \\ (+Bp_1 - x(t))GB & -\frac{SR}{GB} \leq +Bp_1 - x(t) \leq +\frac{SR}{GB} \\ -SR & + Bp_1 - x(t) < -\frac{SR}{GB} \end{cases}$$

$$p_2 = \begin{cases} +SR & - x(t) > +\frac{SR}{GB} \\ -x(t)GB & -\frac{SR}{GB} \leq -x(t) \leq +\frac{SR}{GB} \\ -SR & - x(t) < -\frac{SR}{GB} \end{cases}$$

$$p_3 = \begin{cases} +SR & - Bp_1 - x(t) > +\frac{SR}{GB} \\ (-Bp_1 - x(t))GB & -\frac{SR}{GB} \leq -Bp_1 - x(t) \leq +\frac{SR}{GB} \\ -SR & - Bp_1 - x(t) < -\frac{SR}{GB} \end{cases}$$
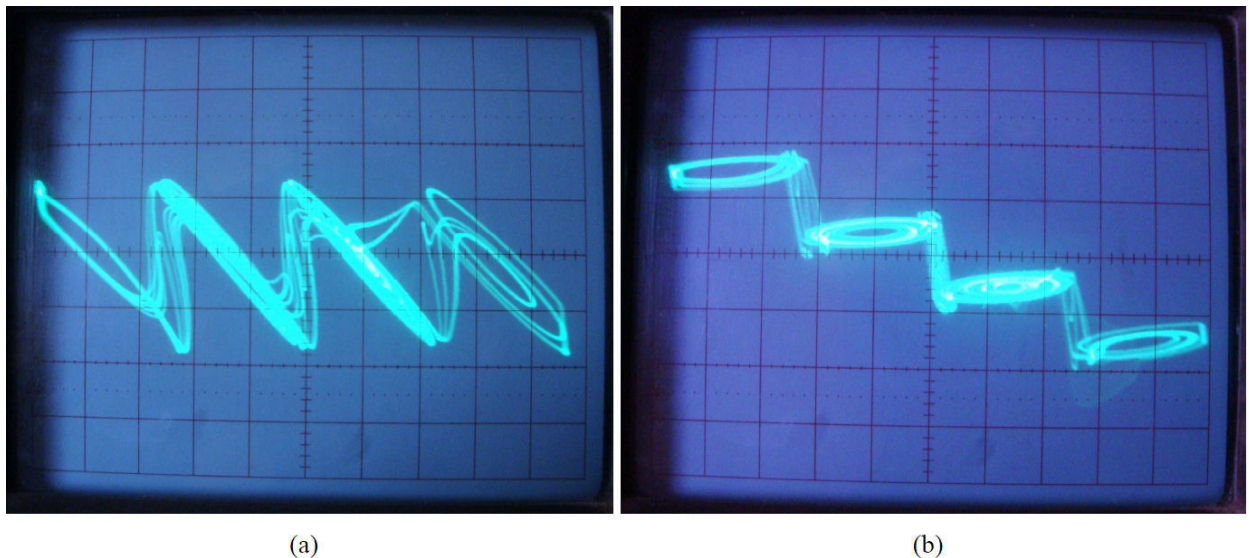
(8)

FIGURE 6. Experimental verification of 4-scroll attractor. Vertical axes: 20 mV/div; Horizontal axes: 2 V/div (a) *x(t)-z(t)* plane, (b) $x(t) - V_s(x)$ plane, where $V_s(x) \approx i(x)R_s$.

TABLE II. Component list from Fig. 5.

Element	Value	Tolerance
Opamps	UA741AN	
R	10 kΩ	$\pm 5\%$
R_s	500 Ω Potentiometer	
$R_{1,2,3}$	40 kΩ	$\pm 5\%$
$R_{x,y,z}$	10 kΩ	$\pm 5\%$
$R_{x2,y2}$	7 kΩ	$\pm 5\%$
$C_{x,y,z}$	5.84 nF (for 3.45 kHz)	$\pm 5\%$
$\pm B_p$	$\pm$ 4.5 V	

According to Fig. 5 and (8), chaotic waveforms can numerically be obtained with a better accuracy compared with PWL models. Table II gives the numerical values of the passive elements used in the experimental tests. In this way, Fig. 6(a) shows experimental results corresponding to $x(t) - z(t)$ plane. It is worth noting that R_s was introduced to indirectly measure $i(x)$ in relation to the chaotic excitation signal, and its value is slightly increased in order to obtain the chaotic attractors shown in Fig. 6(b). From Fig. 6 one can see that the introduction of R_s does not modify drastically the behavior of the chaotic circuit, because its value is small. Note that the representation of the chaotic attractors on the $x(t) - V_s(x)$ plane, where $V_s(x) \approx i(x)R_s$, is reported herein for the first time in the literature.

In short, the use of simple and accurate models that take into account performance parameters of Opamps are very useful to enhance the behavior of continuous nonlinear functions, *e.g.* the SNFS based on Opamps. But even, other continuous nonlinear functions can also be modeled by simply identifying the manner of interconnecting the behavioral models of the Opamps [5,11,17,18,33,34,38,41]. Therefore, the numeric generation of multi-scrolls chaotic attractors, not only at 1-D, but also at 2-D, 3-D and 4-D can be better predicted. Finally, we also remark that to the best knowledge of the authors, the real behavior of the SNFS based on Opamps has not been reported in the literature, until today. In Ref. 29, numeric simulations are only shown, hence, comparisons with similar proposals cannot be done. We would like to note that this work is a great contribution to study and generate chaotic waveforms faster and accurate. As a consequence, topics on the automatic synthesis of chaotic attractors [26,28,40], the synchronization schemes used in communication systems based on chaos [4,10,23,31] and the common metrics used to evaluate the complexity of nonlinear systems [1,8,9,12,20,27,30,32] can be inevitably improved by using the proposed behavior models for Opamps and particularly the SNFS.

6. Conclusions

Real effects on the frequency behavior of the SNFS designed with Opamps have been presented. These effects are more evident when the center frequency of the chaotic excitation signal is increased. By reducing the value of the discrete capacitors in Fig. 5, the center frequency of the chaotic signal is pushed to high-frequency. Therefore, it is clear that the use of PWL models are only feasible at low frequency. A nonlinear behavior model for the SNFS designed with Opamps has been built, where the most influential performance parameters associated to amplifiers have been taken into account. In this context and for comparison purposes, a linear model for the Opamp has been used to obtain the behavior of the SNFS. However, as has been shown throughout the paper, the linear model introduces a high level of inaccuracy compared with the nonlinear model. Furthermore, the availability of a behav-

ioral model, simple and accurate, can impact the computational cost during the generation of multiscroll chaotic attractors, issue that has been not addressed in this paper. Experimental data using commercial available Opamps for generation of the SNFS and 4-scroll attractors were gathered showing good agreement with numerical approximations. Furthermore, voltage comparators with better performance parameters than the UA741 can be used to build the SNFS, however, they are also limited by the *DR*, *GB*, A_{DC} and *SR*, and the behavior of the SNFS shown in Fig. 2(b) will be again observed, but now at higher frequencies. Finally, we remark that the proposed SNFS model can not only be used in the automatic synthesis of chaotic attractors, but also to improve the synchronization schemes widely used in communication systems based on chaos and to achieve a better forecast on the metrics used to evaluate the complexity of a chaotic system.

7. Acknowledgments

1. H.D.I. Abarbanel, R. Brown, and M.B. Kennel, *J. Nonlinear Science* **1** (1991) 25.

2. L.O. Chua and P.M. Lin, *Computer-Aided Analysis of Electronic Circuits: Algorithms and Computational Techniques.* (N.J. Prentice Hall, USA 1975)

3. G. Chen, *Controlling Chaos and Bifurcations in Engineering Systems* (Boca Raton, Florida, CRC Press LLC, USA 1999)

4. G. Chen and T. Ueta, *Chaos in Circuits and Systems* (World Scientific Publishing Co. Pte. Ltd., Singapore 2002)

5. D. Chen Z. Sun, X. Ma, and L. Chen, *Int. J. Circuit Theory Appl.*, Doi: 10.1002/cta.1860 (2012).

6. A.S. Elwakil and M.P. Kennedy, *IEEE Trans. on Circuits Syst. I, Fundam. Theory Appl.* **47** (2000) 4.

7. A.S. Elwakil, K.N. Salama, and M.P. Kennedy, *Int. J. Bifurc. Chaos* **12** (2002) 11.

8. F.I. Fazanaro, D.C. Soriano, R. Suyama, R. Attux, M.K. Madrid, and J.R. Oliveira, *Chaos* **23** (2013) 10.

9. P. Grassberger and I. Procaccia, *Physical Review A* **28** (1983) 3.

10. L. Gámez-Guzmán, C. Cruz-Hernández, R. López-Gutiérrez, and E. García-Guerrero, *Application to communication. Commun. Nonlinear Sci. Numer. Simul.* **14** (2009) 11.

11. T. Gotthans and Z. Hrubos, *J. Elect. Eng.* **64** (2013) 5.

12. J.A. Hernández, R.M. Benito, and J.C. Losada, *Int. J. Bifurc. Chaos* **21** (2011) 11.

13. A. Khan and P. Singh, *Int. J. Bifurc. Chaos* **18** (2008) 7.

14. J. Lü, G. Chen, X. Yu, and H. Leung, *IEEE Trans. CAS-I* **51** (2004) 15.

15. J. Lü and G. Chen, *Int. J. Bifurc. Chaos* **16** (2006) 84.

16. J. Lü, S. Yu, H. Leung and G. Chen, *IEEE Trans. CAS-I* **53** (2006) 17.

17. X. Liu, X. Shen, and H. Zhang, *Int. J. Bifurc. Chaos* **22** (2012) 15.

18. Y. Liu, S. Pang, and D. Chen, *Math. Comp. Mod.* **57** (2013) 21.

19. S. Ozoguz *et al.*, *Electron. Lett.* **38** (2002) 2.

20. S. Rugonyi and K.J. Bathe, *Int. J. Numerical Methods in Engineering* **56** (2003) 19.

21. A.G. Radwan, A.M. Soliman, and A. El-Sedeek, *IEEE Trans. Circuits Syst. I, Fundam. Theory Appl.* **50** (2003) 4.

22. J.A.K. Suykens and J. Vandewalle, *IEEE Trans. CAS-I* **40** (1993) 8.

23. H. Sira-Ramírez and C. Cruz-Hernández, *Int. J. Bifurc. Chaos* **11** (2001) 15.

24. C. Sánchez-López, A. Castro-Hernández, and A. Pérez-Trejo, *IEICE Electron. Express* **5** (2008) 5.

25. C. Sánchez-López, R. Trejo-Guerra, J.M. Muñoz-Pacheco, and E. Tlelo-Cuautle, *Nonlinear Dynamics* **61** (2010) 11.

26. C. Sánchez-López, *Applied Mathematics and Computation* **217** (2011) 9.

27. C. Sánchez-López, J.M. Muñoz-Pacheco, E. Tlelo-Cuautle, V.H. Carbajal-Gómez, and R. Trejo-Guerra, *In: Proc. IEEE Int. Symp. Circuits Syst.* (Rio do Janeiro, Brazil, 2011) p. 2950.

28. C. Sánchez-López, *Rev. Mex. Fis.* **58** (2012) 8.

29. C. Sánchez-López *et al.*, *In Proc. IEEE Int. Latin American Symp.* (Circuits Syst. Cusco, Peru, 2013). p. 1-4

30. H. Shao-Bo, S. Ke-Hui, and Z. Cong-Xu, *Chin. Phys. B* **22** (2013) 6.

31. R. Trejo-Guerra, E. Tlelo-Cuautle, C. Cruz-Hernández, and C. Sánchez-López, *Int. J. Bifurc. Chaos* **19** (2009) 10.

32. R. Trejo-Guerra, E. Tlelo-Cuautle, J.M. Muñoz-Pacheco, C. Sánchez-López, and C. Cruz-Hernández, *Int. J. Nonlinear Sciences & Numerical Simulation* **11** (2010) 8.

33. F.Q Wang and C.X Liu, *Int. J. Modern Physics* **22** (2008) 7.

34. C.H. Wang, H. Xu and F. Yu, *Int. J. Bifurc. Chaos* **23** (2013) 10.

35. M.E. Yalcin, J.A.K. Suykens, and J. Vandewalle, *IEEE Trans. Circuits Syst. I, Fundam. Theory Appl.* **47** (2000) 5.

36. M.E. Yalcin, S. Özoguz, J.A.K. Suykens, and J. Vandewalle, *Electron. Lett.* **37** (2001) 2.

37. M.E. Yalcin, J.A.K. Suykens, J. Vandewalle, and S. Özoguz, *Int. J. Bifurc. Chaos* **12** (2002) 19.

38. S.M. Yu, J. Lü, H. Leung, and G. Chen, *IEEE Trans. Circuits Syst. I, Fundam. Theory Appl.* **52** (2005) 19.

39. S. Yu, W.K.S. Tang, and G. Chen, *Int. J. Bifurc. Chaos* **17** (2007) 14.

40. G. Zhong, K.F. Man, and G. Chen, *Int. J. Bifurc. Chaos* **12** (2002) 9.

41. H. Zhang, X. Liu, X. Shen, and J. Liu, *Int. J. Bifurc. Chaos* **23** (2013) 17.